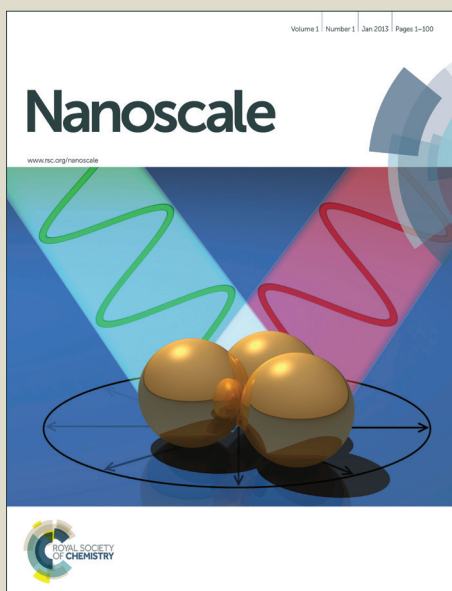


# Nanoscale

Accepted Manuscript



This is an *Accepted Manuscript*, which has been through the Royal Society of Chemistry peer review process and has been accepted for publication.

*Accepted Manuscripts* are published online shortly after acceptance, before technical editing, formatting and proof reading. Using this free service, authors can make their results available to the community, in citable form, before we publish the edited article. We will replace this *Accepted Manuscript* with the edited and formatted *Advance Article* as soon as it is available.

You can find more information about *Accepted Manuscripts* in the [Information for Authors](#).

Please note that technical editing may introduce minor changes to the text and/or graphics, which may alter content. The journal's standard [Terms & Conditions](#) and the [Ethical guidelines](#) still apply. In no event shall the Royal Society of Chemistry be held responsible for any errors or omissions in this *Accepted Manuscript* or any consequences arising from the use of any information it contains.

Cite this: DOI: 10.1039/x0xx00000x

Received 00th February 2014,  
Accepted 00th February 2014

DOI: 10.1039/x0xx00000x

www.rsc.org/

## Decorating Graphene Nanosheets with Electron Accepting Pyridyl Phthalocyanines

Leonie Wibmer,<sup>a</sup> Leandro M. O. Lourenço,<sup>a,b</sup> Alexandra Roth,<sup>a</sup> Georgios Katsukis,<sup>a</sup> Maria G. P. M. S. Neves,<sup>b</sup> José A. S. Cavaleiro,<sup>b</sup> João P. C. Tomé,<sup>b,c\*</sup> Tomás Torres,<sup>d,e\*</sup> Dirk M. Guldi<sup>a\*</sup>

We describe herein the preparation of novel exfoliated graphene-phthalocyanine nanohybrids, and the investigation of their photophysical properties. Pyridyl-phthalocyanines (Pcs) **1-3** are presented as novel electron accepting building blocks of variable strengths with great potential for the exfoliation of graphite *via* their immobilization onto the basal plane of graphene in dimethylformamide (DMF) affording single layer and turbostratic graphene based **G1-G3**. **G1-G3** were fully characterized (AFM, TEM, Raman, steady-state and pump probe transient absorption spectroscopy) and were studied in terms of electron donor-acceptor interactions in the ground and excited state. In this context, electron transfer upon photoexcitation from graphene to the electron accepting Pcs with dynamics, for example, in **G2** of <1 and 330 ± 50 ps for charge separation and charge recombination, respectively, was corroborated in a series of steady-state and time-resolved spectroscopy experiments.

### 1. Introduction

Since the pioneering work by *Novoselov et al.* graphene is one of the first two-dimensional (2D) atomic crystals, which is readily available.<sup>1,2</sup> An overwhelming number of its properties including mechanical stiffness,<sup>3,4</sup> strength, and elasticity – a Young's modulus of 1 TPa and intrinsic strength of 130 GPa –<sup>5,6</sup> electrical and thermal conductivity – above 3,000 W.mK<sup>-1</sup> –<sup>7</sup> etc. are simply outstanding, especially when compared and contrasted to conventional materials. Taking the aforementioned into concert, graphene bears great promises to replace existing materials in emerging applications.<sup>8</sup>

To meet the full potential of graphene, in general, and the requirements for specific applications, in particular, dozens of methods for preparing graphene – featuring various dimensions, shapes and quality – are either in use or under development.<sup>9</sup> A leading example is the micromechanical exfoliation of graphite, which yields high-quality single-layer graphene with room-temperature electron and hole mobility up to 15000 cm<sup>2</sup>/Vs,<sup>10</sup> but comes short of scalability.

Alternatively, bottom-up fabrication strategies of graphene by means of, for example, epitaxial growth<sup>11,12</sup> and/or chemical vapor deposition<sup>13</sup> opened the doors for technological applications. The latter reach from transparent conductive layers,<sup>14</sup> to photonics<sup>15</sup> and nanoelectronics.<sup>16</sup> Only a few substrates such as copper etc. are, however, suitable for the

growth of graphene films and a fairly problematic transfer step is required to facilitate combination with other materials.<sup>17</sup>

In stark contrast, liquid-phase exfoliation of graphite is a widespread method that bears great potential for mass-production of graphene.<sup>18</sup> Liquid-phase exfoliation is currently been conducted in the area of coatings,<sup>19</sup> composites,<sup>20</sup> conductive inks,<sup>21</sup> transparent conductive layers,<sup>22</sup> and energy generation / storage.<sup>23</sup> As such, it is based on bringing graphite with the aid of sonication into contact with a solvent, which, in turn, assists in disintegrating graphite into individual platelets. Exfoliation efficiencies and yields are, however, rather moderate in pure solvents, due to high activation barriers and high thermodynamic stabilities of graphite.<sup>17,24,25</sup>

Somewhat related is the approach of transforming graphite into graphite oxide by means of harsh oxidation, dispersing the resulting flakes by sonication, and reducing it back to graphene.<sup>26</sup> Although this method guarantees processability, on one hand, and covalent functionalization, on the other, it comes along with a significant alteration of the physico-chemical properties of pristine graphene.<sup>27-29</sup> To avoid such setbacks and to secure the efficient exfoliation of graphite the necessity of employing molecular building blocks in the form of amphiphilic intercalators has evolved.<sup>30,31</sup>

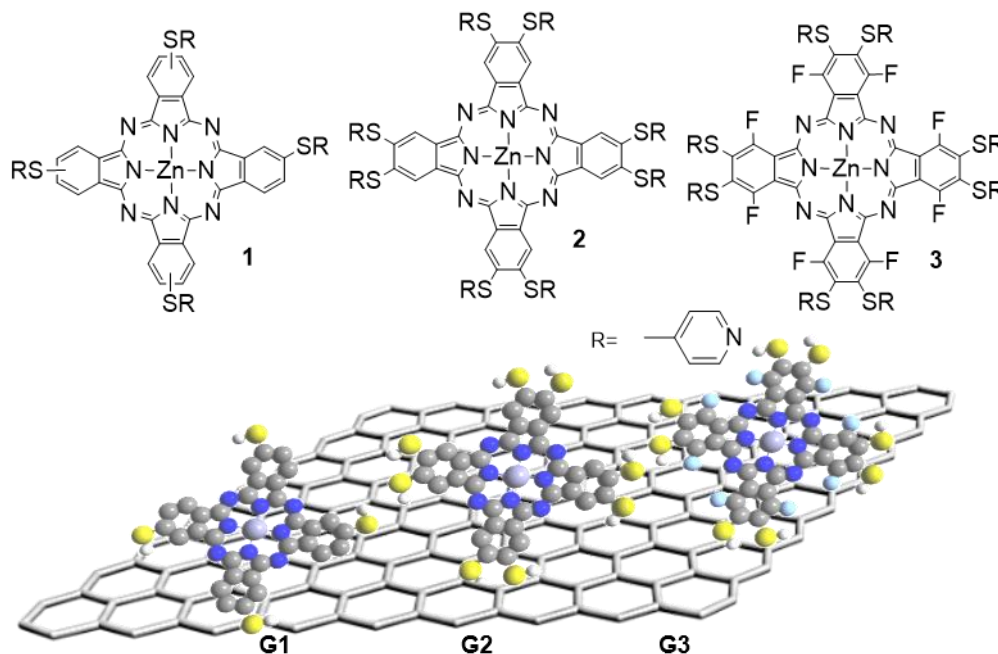
One of the key aspects in graphene research is to tune its electronic properties by chemical doping with molecular

building blocks, while preserving its unique band structure.<sup>32</sup> Importantly, covalent methodologies impact the electronic structure of graphene and, in turn, potentially reduce the charge carrier mobility. On the contrary, non-covalent strategies not only tune the electronic properties of graphene but also minimize the damage to the  $sp^2$ -conjugated lattice.<sup>33</sup> Here, relevant advances are particularly in the area of self-ordering/self-assembling,<sup>34</sup>  $\pi$ -stacking,<sup>35</sup> as well as charge transfer<sup>36</sup> interactions. Such an approach is particularly useful to link photo- and/or redoxactive chromophores<sup>37</sup> to graphene, and, thereby, adding light harvesting and electron transfer features.<sup>38-40</sup> To this date, a fairly large number of molecular building blocks, such as porphyrins,<sup>27</sup> porphycenes,<sup>30</sup> phthalocyanines,<sup>31,41,42</sup> perylenes, etc. have successfully been immobilized onto the basal plane of graphene.

In the current study, we focus on phthalocyanine/graphene nano hybrids<sup>43,44,45,46,47-49</sup> as promising electron donor-acceptor building blocks in, for example, solar energy conversions schemes. This constitutes a contemporary research topic,

especially in terms of producing innovative materials of greatly reduced sizes. In this context, we report herein the immobilization of pyridyl-appended phthalocyanines **1-3** (Scheme 1) onto graphene. The unique absorption features of phthalocyanines throughout the solar spectrum render them well suited for our approach. And, furthermore, the newly synthesized pyridyl phthalocyanines show, in contrast to the standard tetra *tert*-butyl substituted phthalocyanine (**ZnPc**), electron accepting properties, especially in combination with exfoliated graphite.

Usually, phthalocyanines are poorly soluble and tend to aggregate in many solvents. But, with an adequate selection of peripheral substituents these disadvantages may be minimized/overcome.<sup>50</sup> The synthesis of all the target compounds follows previous procedures already reported by us.<sup>51</sup>



**Scheme 1.** Structures of pyridyl-phthalocyanines **1-3** and corresponding graphene-phthalocyanine hybrids **G1-G3**.

## 2. Experimental

### 2.1. Optical characterization.

Steady-state absorption spectra were recorded with a Perkin-Elmer Lambda 35 and a Perkin-Elmer Lambda 2. Steady-state emission spectra were recorded with a Fluoromax-3-spectrometer from HORIBA JobinYvon. All samples were measured in a fused quartz cuvette with a diameter of 10 mm.

### 2.2. Femtosecond transient absorption spectroscopy.

Femtosecond transient absorption spectra were obtained with a Ti:sapphire laser system CPA-2101 (Clark-MXR, Inc.) in combination with a Helios TAPPS detection unit from Ultrafast Inc.

The initial laser excitation wavelength is 775 nm with a pulse width of 150 fs. The used excitation wavelength was 387 nm, which was generated with a SHG crystal. For the generation of the white light a sapphire crystal of adequate thickness was used. The chirp-effect between 420 and 770 nm is approximately 350 fs. The detection was carried out with two CCD cameras, each for a specific measuring range. The spectral window is therefore 415 to 770 nm and 770 to 1600 nm. The delay line allows spectral acquisition up to time delays of 8000 ps. All samples were measured in a fused quartz cuvette with a thickness of 2 mm. Data was acquired with the software HELIOS Visible/nIR (Newport / Ultrafast Systems).

### 2.3 Electrochemical characterization.

For electrochemistry, a Teflon coated Pt wire was used as working electrode, a Pt wire as counter electrode, and an Ag-wire as quasi reference electrode. For better comparison the potentials were then converted to a ferrocene/ferrocenium redox couple. For spectroelectrochemistry, a Pt net was used as working electrode, a Pt sheet as counter electrode, and an Ag wire as quasi reference electrode. As electrolyte 0.1 M tBAPF<sub>6</sub> (Tetrabutylammonium hexafluorophosphate) was used. The potentials were applied with a METROHM PGSTAT 101 and the absorption spectra taken with a UV/nIR Cary5000 spectrometer.

#### 2.4. Raman spectroscopy.

Raman measurements were carried out with a Renishaw inVia Reflex Confocal Raman Microscope using laser excitations of 532 nm. The sample was prepared by drop casting a dispersion on a Si substrate with a 300 nm oxide layer.

#### 2.5. Transmission electron microscopy.

Sample preparation was performed by drop casting and drying the hybrids on lacey carbon coated copper grids. Bright-field TEM images were recorded with an 80 kV EM 900 from Carl Zeiss AG.

#### 2.6. Atomic force microscopy.

AFM images were obtained with a NanoscopeIIIa Multimode, Veeco in tapping mode. The sample was prepared by drop casting a dispersion on a Si substrate with a 300 nm oxide layer.

### 3. Results and Discussion

Initial measurements regarding the ground and excited state features of **1-3** were performed in DMF – see upper part of Figure 1. From the fairly narrow Q-bands at 10<sup>-6</sup> M, we deduce the lack aggregation of **1-3** at the tested concentrations. In DMF, evidence for monomeric **1-3** are Q-band maxima at 684, 703, and 722 nm. Interestingly, as the number of substituents at the β-position increases the Soret- and the Q-bands shift bathochromically. The lower part of Figure 1 shows the fluorescence spectra of monomers of **1-3** upon excitation at 630 nm in DMF. They reveal maxima at 689, 710, and 730 nm. The quantum yields are 0.23, 0.18, and 0.12 for **1**, **2**, and **3**, respectively, and with that slightly lower than the quantum yield of 0.3 seen for the **ZnPc** reference.<sup>52</sup>

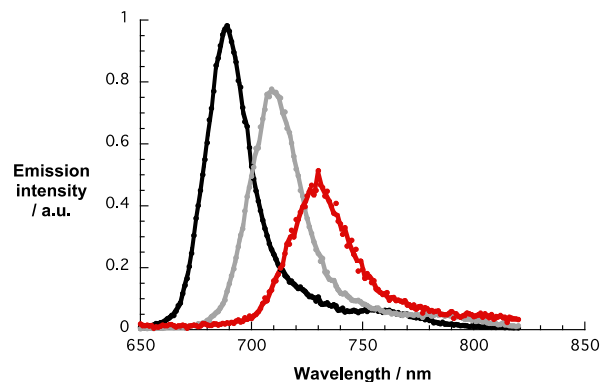
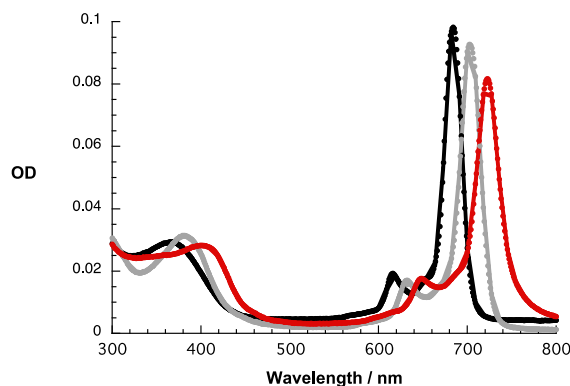


**Figure 1.** Upper part – absorption spectra of **1** (black spectrum), **2** (grey spectrum), and **3** (red spectrum) in DMF; Lower part – fluorescence spectra, upon excitation at 630 nm, of **1** (black spectrum), **2** (grey spectrum), and **3** (red spectrum) in DMF at concentrations of 10<sup>-6</sup> M.

As a complement, Time-Correlated Single Photon Counting (TCSPC) measurements were performed following 403 nm excitation – Figure S1 in the supporting information. The resulting fluorescence time profiles for the pyridyl-phthalocyanines are best fit monoexponentially. The resulting lifetimes are 2.5 ns for **1**, 2.1 ns for **2**, and 1.9 ns for **3**.

Next, transient absorption spectra following 387 nm femtosecond excitation of **1-3** and **ZnPc** were recorded. Right after the excitation of, for example, **2**, the differential absorption characteristics of the singlet excited state are discernable – Figure 2. These are minima, which evolve at 632 and 705 nm, and, which are ascribed to ground state bleaching in the range of the Q-band transitions, as well as 500, 840, and 1200 nm maxima. The singlet excited state is, however, metastable and during its decay a notable red-shift of the maximum, that is, from 500 to 524 nm, is seen. As such, the underlying trend reflects the superimposition of two different transients driven by intersystem crossing. On one hand, it is the decaying singlet excited state. On the other hand, it is the concurrently developing triplet excited state with maxima at 524, 564, and 605 nm. Analyses of the absorption time profiles at 500 nm, etc. shed light onto the kinetics. In particular, a short lifetime of 10 ± 0.8 ps, a long lifetime of 2.7 ± 0.3 ns, and an intermediate lifetime with a minor amplitude of 250 ± 60 ps correlate with internal conversion, intersystem crossing, and the presence of aggregates, respectively. The lifetime of the triplet excited state exceeds the time resolution of our experimental setup. A quantitatively similar behavior is noted for **1**, **3**, and also **ZnPc**. The only differences are slightly altered lifetimes – Figure S2.

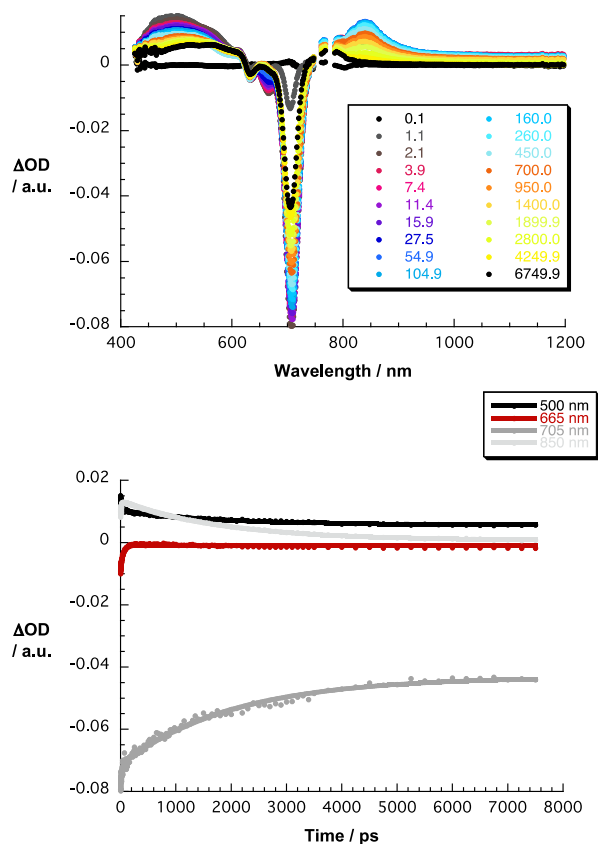


**Figure 2.** Upper part – differential absorption spectra (visible and near infrared) obtained upon femtosecond pump probe experiments (387 nm) of **2** in DMF with time delays between 0.1 and 6750.1 ps at room temperature – for time delays see figure legend. Lower part – time absorption profiles of the spectra shown at 500, 665, 705, and 850 nm.

In addition to the spectroscopic characterization, **1-3** were characterized by electrochemical techniques in DMF – Figure S3. In terms of reductions, the reduction potentials are -1.22 V for the first one followed by a second reduction at -1.56 V for **1**, -1.04 V and -1.28 V for **2**, and -0.86 V and -1.25 V for **3**. In terms of oxidation, only for **1** an oxidation potential was noted at +0.51 V, for **2** and **3** within the experimental range of our measurements, namely up to 0.62 V, no oxidation potential was found. An extrapolation from absorption data gives oxidation potentials of approximately +0.7 and +0.9 V for **2** and **3**, respectively. In this respect, the choice of different solvents including DMSO, THF or – in addition of 4-(dimethylamino)-pyridin for guaranteeing monomeric phthalocyanines – dichloromethane, and an acetonitrile/toluene (3/1 v/v) mixture did not change the results. In contrast, tetra-*tert*-butylphthalocyanine (**ZnPc**) revealed a reduction at -1.43 V and oxidation at +0.24 in DMF.

As a complement, spectroelectrochemical assays were performed in DMF. In the case of **2**, applying a voltage of -0.4 V vs Ag-wire leads to changes in the absorption spectra, which are ascribed to the formation of the one electron reduced phthalocyanine. In particular, next to the bleaching of the

Soret- and Q-bands, new maxima in the visible region at 467, 594, and 740 nm as well as in the near infrared region at 876, 913, 952, and 1000 nm arise in the differential absorption spectra – Figure 3. For **1** and **3**, similar results are noted at, however, slightly different potentials – Figures S4 and S5. For example, the signature of the one electron reduced phthalocyanine of **1** evolves at an applied potential of -0.6 V vs Ag-wire. For **3**, an applied potential of only -0.2 V vs Ag-wire is sufficient to form the one electron reduced phthalocyanine, while at -0.6 V its two electron reduced form is generated. In other words, the electron accepting properties scale with increasing number of substituents at the  $\beta$ -position of the phthalocyanine. Interestingly, no appreciable changes in the absorption spectra were seen upon applying positive voltages in any of the used solvents. For **ZnPc**, in contrast, a spectroelectrochemical oxidation was possible in dichloromethane at an applied potential of 0.5 V. Here, features at 411, 525, 835, and 916 nm are due to the characteristic and well known signature of the one electron oxidized phthalocyanine.

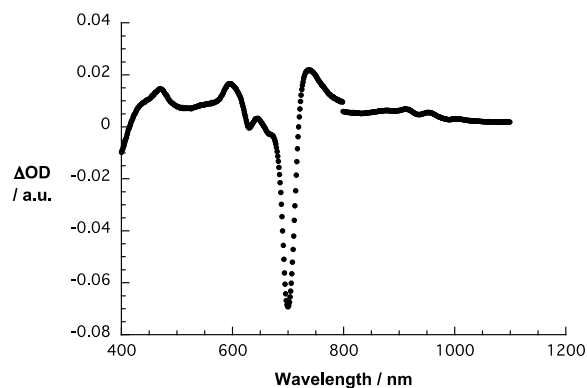


**Figure 3.** Differential absorption spectrum (visible and near infrared) obtained upon spectroelectrochemical one electron reduction of **2** in DMF with a voltage of -0.4 V vs Ag wire.

Having established the key features of **1-3**, we turned to the preparation of the respective nanographene/Pc nanohybrids **G1-G3**, and, as comparison, also **GZnPc** following a previously reported procedure.<sup>53</sup> In particular, 1-2 mg of natural graphite were added to a  $10^{-5}$  M DMF solution of pyridylphthalocyanines, which were ultrasonicated for 45 min and subsequently centrifuged at 20 G for 20 min. The supernatants were then extracted and again subjected to ultrasonication with newly added natural graphite.

Absorption spectra were recorded after each enrichment cycle and compared to those of a control, that is, the corresponding references. Overall, an increase in absorbance is discernable with each enrichment cycle when using **G1-G3** as well as **GZnPc** with equal contributions from absorption and scattering processes of exfoliated graphite. Notably, the exact amount of exfoliated graphite cannot be calculated due to superimposing absorption features of exfoliated graphite and **G1-G3**. The absorption spectra of **GZnPc** lack, however, any additional changes. In contrast, new absorption features evolve for **G1-G3**, which intensify with each enrichment cycle, and, which red shift with respect to the original Q-band. The maxima are at 718, 737, and 760 nm for **G1**, **G2**, and **G3**, respectively –

Figure 4. In the end, the original Q-bands have completely disappeared. Instead, just the new 35 nm red-shifted Q-bands are visible. In the case of **G2**, only four enrichment cycles are necessary – Figure S5 – to obtain the fully shifted Q-band, for **G1** and **G3**, it needs at least 5 to 6 enrichment cycles.

Next to the absorption spectra, fluorescence spectra were recorded. Figure S7 gathers the corresponding fluorescence spectra after each enrichment cycle of **G2**. Please note that after four enrichment cycles the phthalocyanine centered fluorescence is nearly quantitatively quenched – 99.4% in **G1**, 98.6% in **G2**, and 74.8% in **G3**. These trends are in line with the absorption changes seen for **G1-G3** and indicate that at the completion of the enrichment, no free phthalocyanines are present anymore in solution, instead it is mainly immobilized onto graphene. On the contrary, in the case of **GZnPc** only a weak quenching is observed.

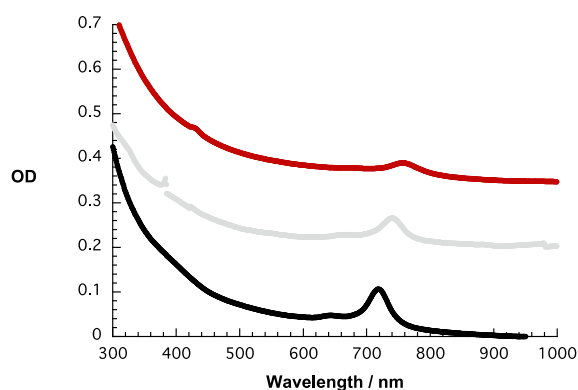


**Figure 4.** Absorption spectra of **G1** (black spectrum), **G2** (grey spectrum), and **G3** (red spectrum) in DMF.

Further insights into the nature of **G2** came from Raman spectroscopy following laser excitation at 532 nm after drop casting the dispersion onto a Si/SiO<sub>2</sub> wafer. Raman spectroscopy is an important mean to characterize graphitic materials and identify single, bi-, and few-layer graphene or turbostratic graphite. Typically, the D-band is discernable at around 1350 cm<sup>-1</sup>, while the G- and 2D-bands are centered around 1580 and between 2650 and 2700 cm<sup>-1</sup>, respectively. Figure 5 shows a selected Raman spectrum of **G2**. The I(2D) / I(G) intensity ratio of 6.3 and a single Lorentzian fit of the 2D-band with a FWHM of 34.6 cm<sup>-1</sup> indicate monolayer graphene. In order to get statistical insights regarding the sample, a Raman map with around 600 different spectra was evaluated – Figure 5. The resulting I(2D) / I(G) intensity ratios are best fit by a log-normal distribution function, which maximizes at a ratio of 0.97. From reference experiments we attribute any ratio of 0.7 or less to bulk graphite or few- to multilayer graphene. That means, in the current case, 25% of the collected spectra reveal bulk graphite / few- to multilayer graphene character, while 75% of the collected spectra correspond to turbostratic exfoliated graphite and monolayer graphene. For a further differentiation between the latter the FWHM of the 2D-band evolves as a decisive criterion. So furthermore, a shape analysis of the 2D-band of the spectra with a 2D/G intensity ratio above 1 was performed. In this case, the spectra could be fit with a single Lorentzian function, but differ in FWHM. On one hand, 5% of the spectra display a FWHM between 25 and

45 cm<sup>-1</sup> representing real monolayer graphene and, on the other hand, 95% turbostratic graphite with a FWHM between 45 and 70 cm<sup>-1</sup>. The high amount of turbostratic graphite is probably due to our preparation method of simply drop casting the dispersion onto the wafer. Hereby, the once exfoliated flakes tend to reagglomerate upon the slow evaporation of DMF.<sup>54</sup>

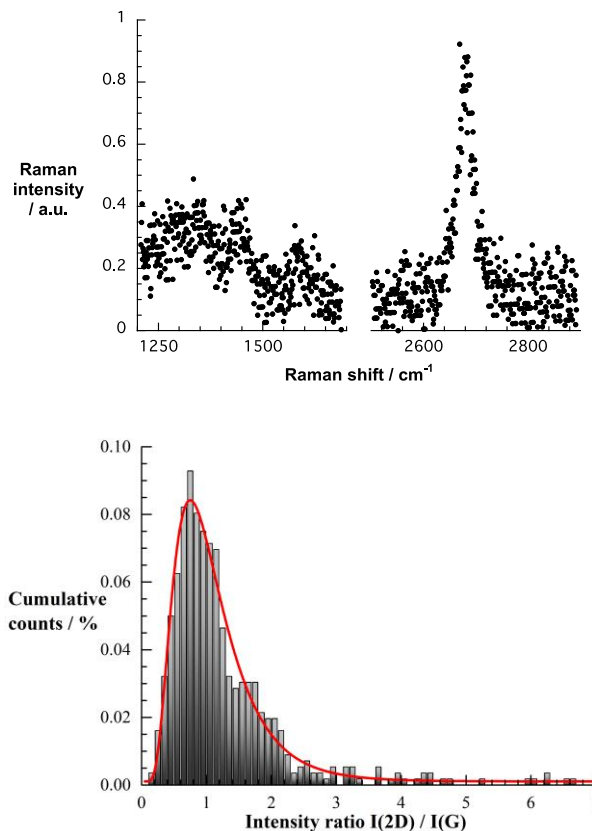


**Figure 5.** Upper part – selected Raman spectrum of **G2**. Lower part – histogram with relative counts vs. I(2D) / I(G) ratio and the corresponding log-normal distribution with a maximum at 0.97. The sample was drop casted from a DMF dispersion onto silicon oxide wafers and was excited at 532 nm.

This is also confirmed by transmission electron microscope images of, for example, **G2** – Figure 6. In particular, small thin flakes, as well as larger individual few-layer graphene flakes with lateral sizes up to 2 μm appear folded and intertwined to minimize surface energy. Furthermore, in atomic force microscopy homogeneous flakes are found onto which smaller flakes as well as graphitic materials agglomerate. Specifically, height profiles of graphene flakes reveal sizes up to 1 μm that are around 1 nm in height, which still corresponds to a monolayer flake due to adsorbed water or stabilizer molecules.<sup>55,56</sup> Agglomerated flakes are again 1 nm in height, whereas height profiles of graphitic materials reach 10 nm and beyond – see Figure 6.

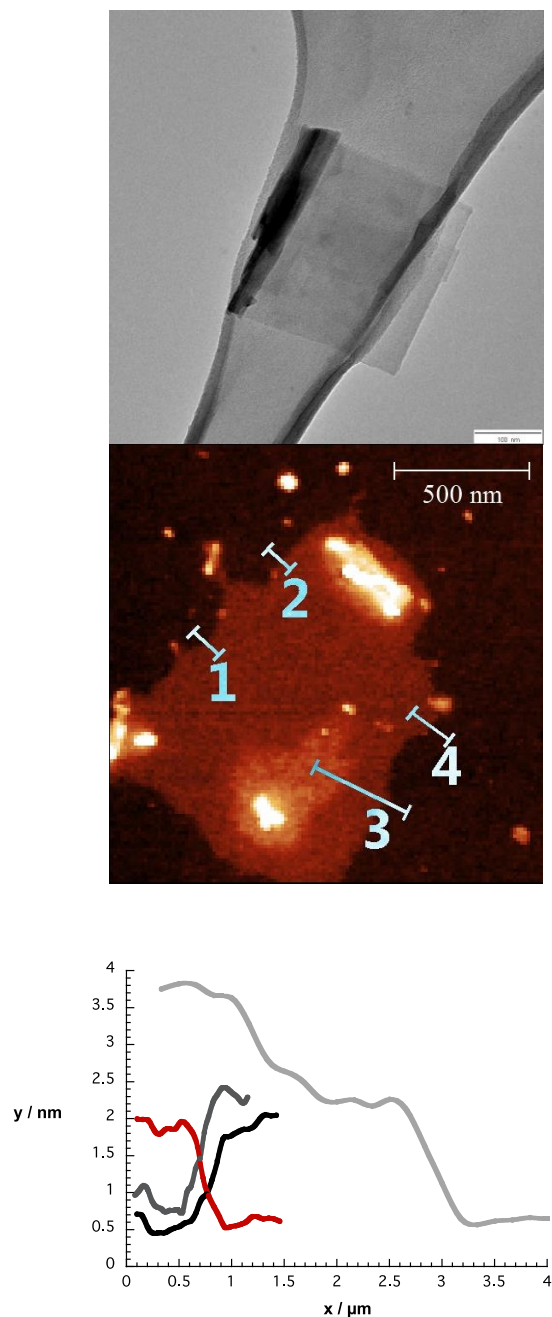


**Figure 6.** Upper part – TEM images of **G2** on a lacey carbon grid – scale bar is 100 nm. Central part – tapping mode AFM image of **G2** on a  $\text{SiO}_2$  surface – scale bar is 500 nm. Lower part – height profiles at positions 1 (black), 2 (dark grey), 3 (light grey), and 4 (red).

Finally, to characterize and to quantify the nature of the electronic interactions between graphene and the phthalocyanines in terms of energy and/or electron transfer, we performed transient absorption experiments with **G1-G3** and **GZnPc** by means of exciting them at 387 nm. In order to obtain better results in the spectroscopic range between 700 and 800 nm, all measurements were carried out with a white light setting that is optimized in this range of the spectrum. In the case of **GZnPc**, the differential absorption spectrum lacks features in addition to those seen for the references, that is, graphene, on one hand, and **ZnPc**, on the other hand – not

shown. With regard to the earlier, a graphene related bleaching is discernable in the range from 900 to 1600 nm. With regard to the latter, the intensity of the phthalocyanines' ground state bleaching, which is seen in the form of minima at 623 and 679 nm prompts to the presence of **ZnPc** that is free in solution and not immobilized onto graphene. Furthermore, the accordingly formed singlet-singlet absorption gives rise to maxima at 506, 592, and 856 nm, respectively, and, as such, identical to what is seen for the reference **ZnPc**.

In stark contrast, in the case of **G2**, within the first picoseconds following excitation broad minima evolve – Figure 7. It comprises graphene related bleaching in the visible and near infrared regions and phthalocyanine related ground state bleaching between 650 and 740 nm. Importantly, the phthalocyanine related ground state bleaching is 35 nm red-shifted in **G2** to 740 nm relative to the spectra recorded for **2**. In fact, the minima for **G2** are in excellent agreement with the shifted Q-band absorption seen in the absorption spectra. Both, that is, graphene and phthalocyanine related bleaching, decay rapidly – *vide infra*. For example, considering the bleaching of graphene at 1035 nm a lifetime of <1 ps evolves. Following the fast decay of these excited states, new features develop in the visible region at 462, 578, and 763 nm. In line with the spectroelectrochemical investigations carried out with **2** in DMF – Figure 3 – the latter features suggest the formation of the one electron reduced form of the phthalocyanine following excited state electron transfer. The near infrared region is equally important. Here, new features were noted during the transient decay with a broad maximum ranging from 950 to 1300 nm. Implicit are new valence band holes in graphene – accepted from photoexcited **2**. Implicit is the formation of radical ion pair states, that is, reduced **2** and oxidized graphene. Analyses at the characteristic wavelengths give rise to three lifetimes, which were best fit by a multi-exponential fitting function affording for **G2** lifetimes of <1 and  $330 \pm 50$  ps for charge separation and charge recombination, respectively. In addition, a 1 ns component, which relates to Q-band ground state bleaching, is derived. Overall, similar results with, however, slightly different spectral features and lifetimes came from complementary studies with **G1** and **G3** as shown in Figures S8 and S9, respectively. Please note that the new absorption features include signals red shifted to the Q-bands. In the case of **G1**, the maximum is found at 742 nm, while for **G3** it is expected to be around 780 nm. The latter is, however, masked by the fundamental of the laser excitation at 775 nm. Interesting is the trend in terms of charge separation and charge recombination. The charge separation for **G1-G3** always occurs in less than 1 ps, but differs in terms of charge recombination: for **G2** the lifetime of the charge separated state is more than twice as long as those found for **G1** and **G3**.

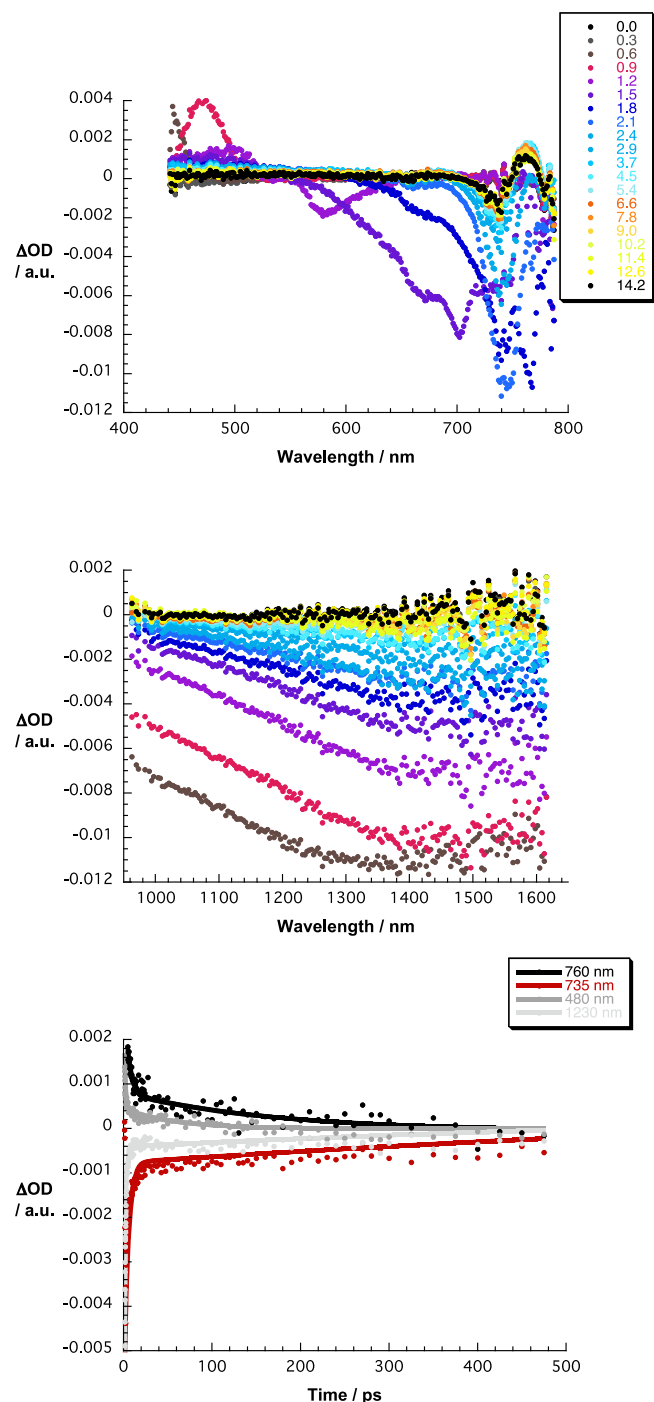


**Figure 7.** Upper part– differential absorption spectra (visible) obtained upon femtosecond pump probe experiments (387 nm) of **G2** in DMF with time delays between 0 and 14.2 ps at room temperature – for time delays see figure legend. Central part – differential absorption spectra (near infrared) obtained upon femtosecond pump probe experiments (387 nm) of **G2** in DMF with time delays between 0 and 14.9 ps at room temperature – for time delays see figure legend of upper part. Lower part – time absorption profiles of the spectra shown at 480, 735, 760, and 1230 nm.

## Conclusions

Pyridyl phthalocyanines **1-3** have been newly synthesized as promising building blocks to exfoliate graphite *via* their immobilization onto the basal plane of graphene. Interestingly, in comparison to the **ZnPc** reference they reveal much lower reduction potentials. As a matter of fact, immobilization of **1-3** to afford electron donor-acceptor nanohybrids **G1-G3** is enabled through electronic coupling as seen in newly developing absorption features and an almost complete quenching of the phthalocyanine fluorescence. The different affinities between Pc **2** and Pc **3** derivatives relative to graphene in **G2** and **G3**, respectively, are likely due to different physico-chemical properties. The aforementioned was complemented by femtosecond pump probe spectroscopy, which corroborated that the electronic coupling between **G1-G3**, on one hand, and graphene, on the other hand, is indeed inception to a charge transfer to generate the one electron reduced phthalocyanine. In **G2**, the dynamics are  $<1$  and  $330 \pm 50$  ps for charge separation and charge recombination, respectively. Raman, TEM, and AFM analysis revealed that after drop casting the dispersion onto a Si/SiO<sub>2</sub> wafer, the exfoliated flakes tend to minimize surface energy by folding or reaggregating, thus forming turbostratic graphene. In stark contrast, control experiments with the **ZnPc** reference corroborated the lack of ability of the latter to exfoliate graphite to any reasonable extent. Our results demonstrate that the pyridines on the Pcs play a decisive role in governing the interactions with the graphene. Recently,<sup>57</sup> theoretical studies have corroborated that the enhanced stability of pyridines on graphene stems from the matches between frontier orbitals of pyridine derivatives and those of graphene. Additional work is, however, needed to gain a full and comprehensive understanding of this kind of interactions.

## Acknowledgements

Thanks are due FCT (Portugal), European Union, QREN, COMPETE and FEDER for funding QOPNA Research Unit (Project PEst-C/UI0062/2013) and projects PTDC/CTM/101538/2008 and PTDC/UI/65228/2006. Support is also acknowledged from the Spanish MEC and MICINN (CTQ2011-24187/BQU and PRI-PIBUS-2011-1128), and the Comunidad de Madrid (S2013/MIT-2841 FOTOCARBON). Leandro M. O. Lourenço thanks FCT for his PhD grant (SFRH/BD/64526/2009).

## Associated content

**Supporting Information.** Additional information as noted in the text. This material is available free of charge via the Internet at <http://pubs.acs.org>.

## Author information

Corresponding Authors

\*[jtome@ua.pt](mailto:jtome@ua.pt); [tomas.torres@uam.es](mailto:tomas.torres@uam.es); [dirk.guldi@fau.de](mailto:dirk.guldi@fau.de)

## Notes and references

<sup>a</sup> Department of Chemistry and Pharmacy and Interdisciplinary Center for Molecular Materials, Friedrich-Alexander-University Erlangen-Nuremberg, 91058 Erlangen, Germany.

<sup>b</sup> QOPNA and Department of Chemistry, University of Aveiro, 3810-193 Aveiro, Portugal.

<sup>c</sup> Department of Organic and Macromolecular Chemistry, Ghent University, B-9000 Gent, Belgium

<sup>d</sup> Department of Organic Chemistry, Autonoma University of Madrid, Cantoblanco, 28049 Madrid, Spain.

<sup>e</sup> IMDEA-Nanociencia, C/Faraday, 9, Cantoblanco, 28049-Madrid, Spain

- <sup>1</sup> K. S. Novoselov, A. K. Geim, S. V. Morozov, D. Jiang, Y. Zhang, S. V. Dubonos, I. V. Grigorieva and A. A. Firsov, *Science*, 2004, **306**, 666–669.
- <sup>2</sup> A. K. Geim and K. S. Novoselov, *Nat. Mater.*, 2007, **6**, 183–191.
- <sup>3</sup> C. Lee, X. Wei, J. W. Kysar and J. Hone, *Science*, 2008, **321**, 385–388.
- <sup>4</sup> J. S. Bunch, S. S. Verbridge, J. S. Alden, A. M. van der Zande, J. M. Parpia, H. G. Craighead and P. L. McEuen, *NanoLett.* 2008, **8**, 2458–2462.
- <sup>5</sup> A. K. Geim, *Science*, 2009, **324**, 1530–1534.
- <sup>6</sup> I. A. Ovid'ko, *Rev. Adv. Mater. Sci.*, 2013, **34**, 1–11.
- <sup>7</sup> V. E. Dorgan, A. Behnam, H. J. Conley, K. I. Bolotin and E. Pop, *NanoLett.*, 2013. DOI: 10.1021/nl400197w.
- <sup>8</sup> R. S. Edwards and K. S. Coleman, *Nanoscale*, 2013, **5**, 38–51.
- <sup>9</sup> K. S. Subrahmanyam, S. R. C. Vivekchand, A. Govindaraj and C. N. R. Rao, *J. Mater. Chem.*, 2008, **18**, 1517–1523.
- <sup>10</sup> Ç. Ö. Girit, J. C. Meyer, R. Erni, M. D. Rossell, C. Kisielowski, L. Yang, C-H. Park, M. F. Crommie, M. L. Cohen, S. G. Louie and A. Zettl, *Science*, 2009, **323**, 1705–1708.
- <sup>11</sup> V. OngunOzcelik, S. Cahangirov and S. Ciraci, *Phys. Rev. B*, 2012, **85**, 235456 (1–7).
- <sup>12</sup> Y. Cai, H. Zhang, J. Song, Y. Zhang, S. Bao and P. He, *Appl. Surf. Sci.*, 2015, **327**, 517–522.
- <sup>13</sup> Y. Zhang, L. Zhang and C. Zhou, *Acc. Chem. Res.*, 2013, **46** (10), 2329–2339
- <sup>14</sup> T. Kobayashi, M. Bando, N. Kimura, K. Shimizu, K. Kadono, N. Umez, K. Miyahara, S. Hayazaki, S. Nagai, Y. Mizuguchi, Y. Murakami and D. Hobara, *Appl. Phys. Lett.*, 2013, **102**, 023112 (1–4).
- <sup>15</sup> F. Bonaccorso, Z. Sun, T. Hasan and A. C. Ferrari, *Nature Photonics*, 2010, **4**, 611–622.
- <sup>16</sup> D. S. Hecht, L. Hu and G. Ir, *Adv. Mater.*, 2011, **23**, 1482–1513.
- <sup>17</sup> X. Li, W. Cai, J. An, S. Kim, J. Nah, D. Yang, R. Piner, A. Velamakanni, I. Jung, E. Tutuc, S. K. Banerjee, L. Colombo and R. S. Ruoff, *Science*, 2009, **324**, 1312–1314.
- <sup>18</sup> Y. Hernandez, V. Nicolosi, M. Lotya, F. M. Blighe, Z. Sun, S. De, I. T. McGovern, B. Holland, M. Byrne, Y. K. Gun'Ko, J. J. Boland, P. Niraj, G. Duesberg, S. Krishnamurthy, R. Goodhue, J. Hutchison, V. Scardaci, A. C. Ferrari and J. N. Coleman, *Nat. Nanotechnol.*, 2008, **3**, 563–568.
- <sup>19</sup> M. Zhang, Y. Ma, Y. Zhu, J. Che and Y. Xiao, *Carbon*, 2013, **63**, 149–156.
- <sup>20</sup> L. Xu, J-W. McGraw, F. Gao, M. Grundy, Z. Ye, Z. Gu and J. L. Shepherd, *J. Phys. Chem. C*, 2013, **117** (20), 10730–10742.
- <sup>21</sup> F. Torrisi, T. Hasan, W. Wu, Z. Sun, A. Lombardo, T. S. Kulmala, G-W. Hsieh, S. Jung, F. Bonaccorso, P. J. Paul, D. Chu and A. C. Ferrari, *ACS Nano*, 2012, **6** (4), 2992–3006.
- <sup>22</sup> X. Li, G. Zhang, X. Bai, X. Sun, X. Wang, E. Wang and H. Dai, *Nat. Nanotechnol.*, 2008, **3** (9), 538–542.
- <sup>23</sup> D. A. C. Brownson, D. K. Kampouris and C. E. Banks, *J. Power Sources*, 2011, **196**, 4873–4885.
- <sup>24</sup> M. Buzaglo, M. Shtein, S. Kober, R. Lovrinčić, A. Vilan and O. Regev, *Phys. Chem.*, 2013, **15**, 4428–4435.
- <sup>25</sup> C. Peng, Y. Xiong, Z. Liu, F. Zhang, E. Ou, J. Qian, Y. Xiong and W. Xu, *Appl. Surf. Sci.*, 2013, **280**, 914–919.
- <sup>26</sup> W. W. Liu and J. N. Wang, *Chem. Commun.*, 2011, **47**, 6888–6890.
- <sup>27</sup> M-E. Ragoussi, J. Malig, G. Katsukis, B. Butz, E. Spiecker, G. de la Torre, T. Torres and D. M. Guldi, *Angew. Chem. Int. Ed.*, 2012, **51**, 6421–6425.
- <sup>28</sup> J. M. Englert, C. Dotzer, G. Yang, M. Schmid, C. Papp, J. M. Gottfried, H-P. Steinrück, E. Spiecker, F. Hauke and A. Hirsch, *Nat. Chem.*, 2011, **3**, 279–286.
- <sup>29</sup> J. Malig, C. Romero-Nieto, N. Jux and D. M. Guldi, *Adv. Mater.*, 2012, **24**, 800–805.
- <sup>30</sup> J. Malig, N. Jux and D. M. Guldi, *Acc. Chem. Res.*, 2013, **46** (1), 53–64.
- <sup>31</sup> W. Brenner, J. Malig, R. D. Costa, D. M. Guldi and N. Jux, *Adv. Mater.*, 2013, **25**, 2314–2318.
- <sup>32</sup> R. D. Costa, J. Malig, W. Brenner, N. Jux and D. M. Guldi, *Adv. Mater.*, 2013, **25**, 2600–2605.
- <sup>33</sup> J. Malig, N. Jux, D. Kiessling, J-J. Cid, P. Vázquez, T. Torres and D. M. Guldi, *Angew. Chem. Int. Ed.*, 2011, **50**, 3561–3565.
- <sup>34</sup> D. M. Guldi and R. D. Costa, *J. Phys. Chem. Lett.*, 2013, **4** (9), 1489–1501.
- <sup>35</sup> G. Katsukis, J. Malig, C. Schulz-Drost, S. Leubner, N. Jux and D. M. Guldi, *ACS Nano*, 2012, **6** (3), 1915–1924.
- <sup>36</sup> J. Malig, A. W. I. Stephenson, P. Wagner, G. G. Wallace, D. L. Officer and D. M. Guldi, *Chem. Commun.*, 2012, **48**, 8745–8747.
- <sup>37</sup> Y. Zhang, P. Ma, P. Zhu, X. Zhang, Y. Gao, D. Qi, Y. Bian, N. Kobayashi and J. Jiang, *J. Mater. Chem.*, 2011, **21**, 6515–6524.
- <sup>38</sup> V. Mani, R. Devasenathipathy, S.-M. Chen, J.-A. Gu and S.-T. Huang, *Renewable Energy*, 2015, **74**, 867–874.
- <sup>39</sup> C. Bikram K. C., S. K. Das, K. Ohkubo, S. Fukuzumi and F. D'Souza, *Chem. Commun.*, 2012, **48**, 11859–11861.
- <sup>40</sup> J. Zhu, Y. Li, Y. Chen, J. Wang, B. Zhang, J. Zhang and W. J. Blau, *Carbon*, 2011, **49**, 1900–1905.
- <sup>41</sup> H. Xu, J. Xiao, B. Liu, S. Griveau and F. Bedioui, *Biosens. Bioelectron.*, 2015, **66**, 438–444.
- <sup>42</sup> S. Pakapongpan, J. P. Mensing, D. Phokharatkul, T. Lomas and A. Tuantranont, *Electrochim. Acta*, 2014, **133**, 294–301.
- <sup>43</sup> J. Malig, N. Jux, D. Kiessling, J.-J. Cid, P. Vázquez, T. Torres and D. M. Guldi, *Angew. Chem. Int. Ed.*, 2011, **50**, 3561–3565.
- <sup>44</sup> G. Bottari, O. Trukhina, M. Ince and T. Torres, *Coord. Chem. Rev.*, 2012, **256**, 2453–2477.
- <sup>45</sup> M.-E. Ragoussi, J. Malig, G. Katsukis, B. Butz, E. Spiecker, G. de la Torre, T. Torres and D. M. Guldi, *Angew. Chem. Int. Ed.*, 2012, **51**, 6421–6425.
- <sup>46</sup> L. Brinkhaus, G. Katsukis, J. Malig, R. D. Costa, M. Garcia-Iglesias, P. Vázquez, T. Torres, and D.M. Guldi, *Small*, 2013, **9**, 2348–2357
- <sup>47</sup> A. Roth, M.-E. Ragoussi, L. Wibmer, G. Katsukis, G. de la Torre, T. Torres and D. M. Guldi, *Chem. Sci.*, 2014, **5**, 3432–3438.

- 
- <sup>48</sup> G. Bottari, G. de la Torre, T. Torres, *Acc. Chem. Res.* 2015, in press.
- <sup>49</sup> M-E. Ragoussi, G. Katsukis, A. Roth, J. Malig, G. de la Torre, D. M. Guldi and T. Torres, *J. Am. Chem. Soc.*, 2014, **136**, 4593–4598.
- <sup>50</sup> L. M. O. Lourenço, A. Hausmann, C. Schubert, M. G. P. M. S. Neves, J. A. S. Cavaleiro, T. Torres, D. M. Guldi and J. P. C. Tomé, *ChemPlusChem*, 2015, DOI: 10.1002/cplu.201500005.
- <sup>51</sup> J. B. Pereira, E. F. A. Carvalho, M. A. Faustino, M. G. P. M. S. Neves, J. A. S. Cavaleiro, N. C. M. Gomes, A. Cunha, A. Almeida and J. P. C. Tomé, *Photochem. Photobiol.*, 2012, **88** (3), 537–547.
- <sup>52</sup> P. S. Vincett, E. M. Voigtand and K. E. Rieckhoff, *J. Chem. Phys.*, 1971, **55**, 4131–4140.
- <sup>53</sup> D. Kiessling, R. D. Costa, G. Katsukis, J. Malig, F. Lodermeier, S. Feihl, A. Roth, L. Wibmer, M. Kehrer, M. Volland, P. Wagner, G. G. Wallace, D. L. Officer and D. M. Guldi, *Chem. Sci.*, 2013, **4**, 3085–3098.
- <sup>54</sup> A. O'Neill, U. Khan, P. N. Nirmalraj, J. Bolandand and J. N. Coleman, *J. Phys. Chem. C*, 2011, **115**, 5422–5428.
- <sup>55</sup> Q. H. Wang, C.-J. Shih, G. L. C. Paulus and M. S. Strano, *J. Am. Chem. Soc.*, 2013, **135**, 18866–18875.
- <sup>56</sup> X. Li, G. Zhang, X. Bai, X. Sun, X. Wang, E. Wang and H. Dai, *Nat. Nanotechnol.*, 2008, **3** (9), 538–542.
- <sup>57</sup> X. Wang, Q. Cai, G. Zhuang, X. Zhong, D. Mei, X. Li and J. Wang, *Phys Chem Chem Phys*, 2014, **16**, 20749–20754.